APL Photonics

Polarization-mediated multi-state infrared system for fine temperature regulation

Cite as: APL Photonics **8**, 030801 (2023); https://doi.org/10.1063/5.0136842
Submitted: 29 November 2022 • Accepted: 19 February 2023 • Accepted Manuscript Online: 20 February 2023 • Published Online: 14 March 2023

Do Hyeon Kim, Se-Yeon Heo, Yeon-Wha Oh, et al.

Polarization-mediated multi-state infrared system for fine temperature regulation

Cite as: APL Photon. 8, 030801 (2023); doi: 10.1063/5.0136842
Submitted: 29 November 2022 • Accepted: 19 February 2023 •
Published Online: 14 March 2023

Do Hyeon Kim,[1] Se-Yeon Heo,[1] Yeon-Wha Oh,[2] Sanghee Jung,[2] Min Hyung Kang,[3] Il-Suk Kang,[2,a)] Gil Ju Lee,[4,a)] and Young Min Song[1,5,a)]

AFFILIATIONS

[1] School of Electrical Engineering and Computer Science, Gwangju Institute of Science and Technology, Cheomdangwagi-ro 123, Buk-gu, Gwangju 61005, Republic of Korea
[2] National Nanofab Center, Korea Advanced Institute of Science and Technology, Daehak-ro 291, Yuseong-gu, Daejeon 34141, Republic of Korea
[3] Korea Electronics Technology Institute, Ballyong-ro 111, Deokjin-gu, Jeonju 54853, Jeollabuk-do, Republic of Korea
[4] Department of Electronics Engineering, Pusan National University, Busandaehak-ro 63, Geumjeong-gu, Busan 46241, Republic of Korea
[5] Artificial Intelligence (AI) Graduate School, Gwangju Institute of Science and Technology, Cheomdangwagi-ro 123, Buk-gu, Gwangju 61005, Republic of Korea

[a)] **Authors to whom correspondence should be addressed:** iskang@nnfc.re.kr; gjlee0414@pusan.ac.kr; and ymsong@gist.ac.kr

ABSTRACT

Passive radiative cooling has been spotlighted as a promising energy-saving cooling technology owing to its energy-free and zero-carbon emission for addressing global energy and climate crises. Although radiative cooling can significantly save cooling energy in hot weather, it inevitably accompanies undesirable cooling in cold weather resulting from a single-state of strong thermal emission. Dual-state emitters have recently been developed for self-adaptive thermoregulation, but they still exhibit energy loss in moderate weather. Herein, we report a "continuous" temperature-regulation system by introducing an infrared (IR) polarization valve as the energy-balancing channel. The proposed scheme controls the emitter temperature simply by the in-plane rotation of the IR polarizer as if closing and opening the valve, which presents heating/cooling capabilities of −17 to 51 W/m^2 and an energy-saving of >20 GJ/year compared with the conventional emitters in all climate zones. Outdoor experiments demonstrate the precise temperature regulation with the range of ΔT_{cool} >2 °C. This proof-of-concept demonstration in the outdoors verifies our approach's reliability, suggesting its applicability in residential buildings, farms, and electronic devices.

I. INTRODUCTION

The global energy and climate crises urgently demand energy saving for net-zero emissions worldwide. From this perspective, eco-friendly thermal management has been essential in all areas, from residential facilities to mobile devices. Conventional thermal regulation technologies, including an air conditioner,[1,2] a furnace,[3] and thermoelectrics[4–6] facilitate accurate temperature control for thermal comfort; however, they require a large energy consumption generated from fossil fuels. Reports have pointed out that energy usage increases by nearly 10% to raise/lower the inner temperature by 1 °C.[7,8] Passive radiative cooling technology has emerged as a promising solution for addressing this issue owing to its advantages of compactness, being energy-free, low cost, and zero-emission.[9–25] High emissivity in the mid-infrared (MIR) atmospheric window enables cooling the objects by drawing their heat and emitting it to cold outer space radiatively. Such novel features have triggered the renaissances of extensive studies on passive radiative cooling, having successful experimental demonstrations, such as solar cells,[26,27] electronic devices,[28,29] buildings,[30,31] clothes,[24,32] and vehicles.[33,34]

The evolutionary approach has considerable potential for saving cooling energy, but it also possesses the possibility to consume substantial heating energy in cold hours or seasons (e.g., winter

and night).[35] Over the past few years, thermal emitters have primarily been focused on reducing heating energy that results from single-emission characteristics. Alternatively, recent studies have presented dual-state emitters that can switch emission spectra for cooling and heating.[11,25,36–40] However, maintaining a precise thermal comfort temperature, particularly in moderate weather (i.e., spring and autumn) that does not require intense cooling or heating, relies on unceasing emissivity adjustment rather than on/off cooling switching. From this perspective, beyond dual-state emitters, multi-state emitters with continuously adjustable emission spectra are attractive candidates for all weather but have been barely studied so far.[41] Active emitters based on phase change materials also provide a thermoregulation function for all seasons; however, they have limitations on customizing the target temperature owing to fixed transition temperatures.[42–45]

Herein, we propose a radiation-based "continuous" temperature-regulation system by introducing a polarization valve, which opens and shuts the energy-balancing channel between an emitter and outer space. The thermal regulation system is composed of a vertically arranged linearly polarized thermal emitter and an IR polarizer. The proposed scheme simply controls the emitter temperature via in-plane rotation of the infrared (IR) polarizer as if closing and opening the valve. Optical simulations find an optimum design of the linearly polarized thermal emitter, which consists of a one-dimensional metal (Ag) grid on a quartz substrate. The proposed system achieves a broad range of emissivity from 2% to 80% with the rotation of the IR polarizer by achieving cross-polarization or co-polarization. Theoretical calculations exhibit the emitter's heating/cooling capabilities (−17 to 51 W/m^2) by adjusting polarization conditions. Building energy analyses evaluate an annual energy saving of up to 20 GJ across all different climate zones when using the proposed temperature regulator on the roof. Outdoor experiments demonstrate the temperature regulation of the emitter within a target temperature range (17–18 °C) by rotating the IR polarizer, confirming the theoretical results.

II. RESULTS AND DISCUSSION

Figure 1(a) illustrates three different types of emitters: single-, dual-, and multi-state emitters. Single-state emitter, corresponding to most thermal emitters, efficiently emits thermal radiation all day due to its single emission spectrum in the MIR region (8–13 μm), resulting in overcooling in certain situations (e.g., nighttime and winter season). Dual-state emitter switches the emissivity spectra at a specific temperature for heating and cooling modes (i.e., high and low thermal emissivity spectra, respectively). This property mitigates an undesired overcooling, which overcomes the limitation of single-state emitters. Nevertheless, the dual-state emitter is not suitable for practical applications, particularly in moderate weather (i.e., spring and autumn), resulting in overcooling or overheating owing to its fixed two emissivity spectra [the graph in (ii) of Fig. 1(a)].

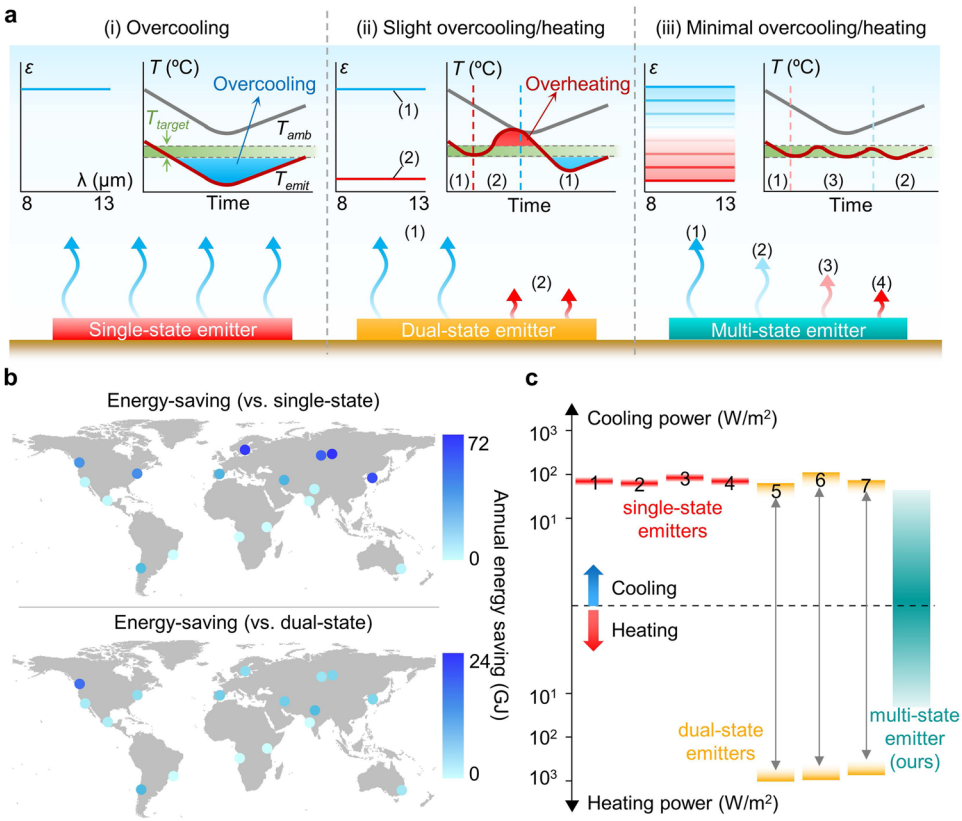

FIG. 1. (a) Comparison of thermal-regulation capabilities between single-, dual-, and multi-state emitters. Green bands of temperature indicate the range of the target temperature. (b) Annual world energy saving of the multi-state emitter compared with different emitter types. (c) Heating/cooling power of polarization-mediated multi-state emitter in comparison with other emitters in the literature.

Compared with the dual-state emitter, the multi-state emitter allows more delicate temperature regulation near the target temperature under the variation of the ambient temperature [the graph in (iii) of Fig. 1(a)]. Continuous variable emission enables fine temperature regulation by responding to the dynamic ambient temperature, effectively preventing the undesired overcooling and overheating.

Figure 1(b) presents the simulated building energy-saving world map based on different climate databases.[46] More details about the simulation method and model appear in Sec. IV and Fig. S1. The multi-state emitter as a roof efficiently reduces the annual energy consumption for thermoregulation in all cities (>20 GJ) than single- and dual-state emitters as roofs. According to a report, to save 20 GJ energy, about a hundred (~100) of HVAC systems should shut down in a month.[47] Consequently, this result implies that the multi-state emitter brings significant economic and environmental benefits in all climate zones owing to its continuous temperature regulation property. In addition, the annual energy consumption saving maps in comparison with a conventional roof present a prominent energy-saving of >50 GJ in all regions, whereas a single-state emitter results in energy wastage in cold regions (Fig. S2). Figure 1(c) shows the heating/cooling performances of our proposed system (-17 to 51 W/m^2) compared with previously reported emitters. This graph manifests the unique benefit of the multi-state emitter with continuous variable emissivity spectra, hence leading to outstanding thermoregulation without overcooling/heating. Detailed information on other emitters, including cooling power and tuning method, appears in Table S1.

Figure 2(a) presents the illustration of our proposed emission regulating system, composed of a linearly polarized thermal emitter and an IR polarizer. A one-dimensional silver (Ag) grating on a quartz (SiO_2) substrate only permits a polarized thermal emission parallel to the Ag grating direction. This is because the electrons in a metal freely move along the metal wires, which blocks the emission with the electric field perpendicular to the Ag grating direction. Thus, the emissivity of the polarization-mediated thermal emitter (PME) varies depending on the polarization angles (φ_{pol}), changing radiation power (P_{rad}), and absorbed radiative power emitted from surroundings (P_{atm}). These two powers maximally decrease by ~100% at a cross-polarization state. In addition, the absorbed solar power (P_{sun}) drops by half owing to a half transmittance of the IR polarizer in the solar region (Fig. S3). The measured emissivity spectra of the fabricated PME at different polarization angles are shown in Fig. 2(b). The polarization dependency of the PME appears from the specific wavelength of 2 μm (dashed line) to the infrared region owing to the optimized grating period (~2 μm). Therefore, the emissivity spectra of the PME exhibit a fine tunability of emissivity (2%–80%) in the MIR region with a negligible change in the solar region with polarization angle change. The measured emissivity spectra of the PME agree well with the calculated results (Fig. S4).

Figure 2(c) shows the optical image and scanning electron microscopy (SEM) images of the fabricated emitter. The sample represents a silvery color owing to little light absorption (~4%). The SEM images show a microscale one-dimensional grating consistent with the proposed design. The detailed fabrication process and design rules of the emitter are given in Sec. IV and Fig. 3. The thermographic images depict the apparent temperature decrease of the fabricated sample as φ_{pol} increases; meanwhile, the sample maintains a fixed actual temperature (50 °C) on the hot plate [Fig. 2(d)]. This exhibits that the amount of outgoing thermal radiation depends on the IR polarizer rotation. Figure 2(e) presents the theoretical cooling performance of the PME at different polarization angles (detailed

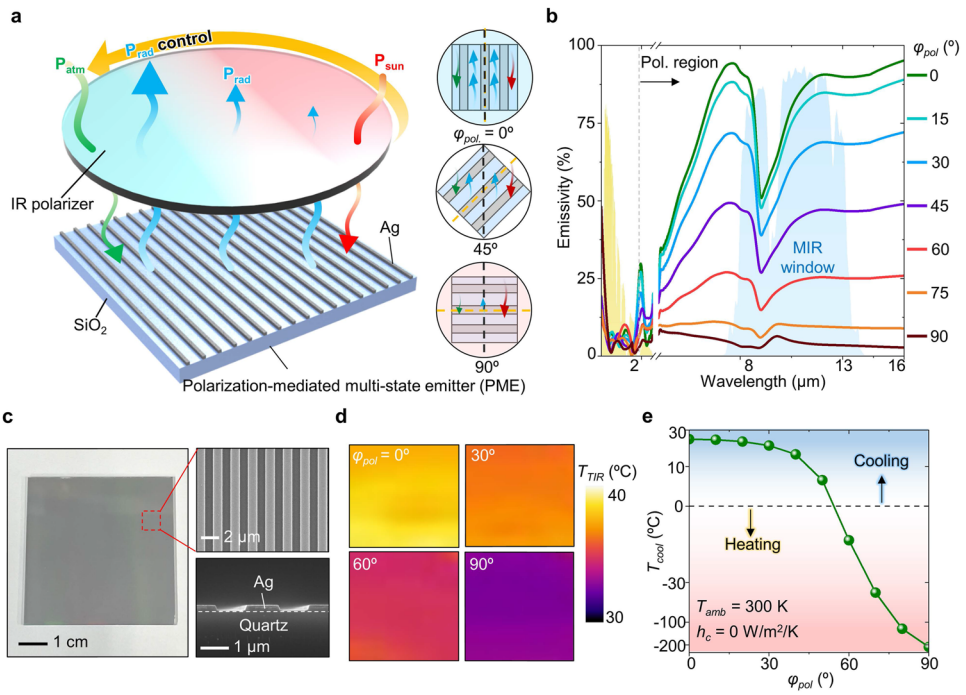

FIG. 2. (a) Schematic of emission modulating system, composed of a polarization-mediated multi-state emitter (PME) and an IR polarizer. (b) Measured emissivity of the PME with different polarization angles. (c) Optical image (left) and SEM images (right) of the fabricated emitter. (d) Thermal images of the fabricated sample under the rotation of a commercial IR polarizer. (e) Calculated cooling temperature of the PME varying with the polarization angles.

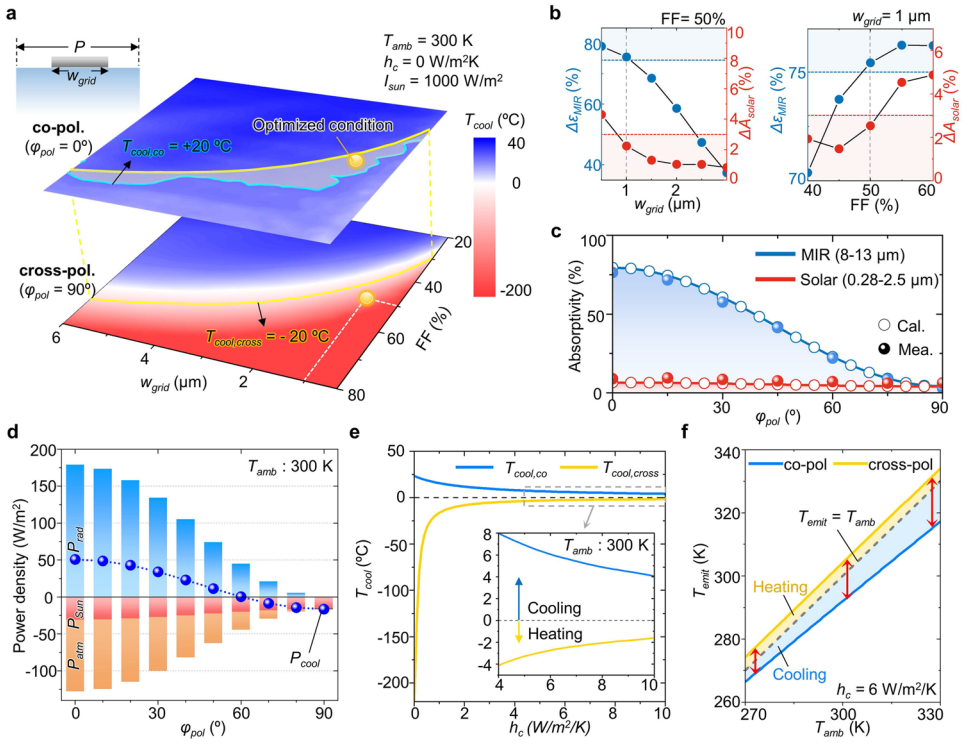

FIG. 3. (a) 3D contour plots for optimization of cooling/heating capability of the PME. (b) Absorptivity differences of the PME in the MIR (8–13 μm) and solar (0.28–2.5 μm) regions as a function of metal grid width (w_{grid}) and metal fill factor (FF). (c) Average absorptivity of the PME at the MIR and solar regions with the variation of polarization angle. Filled and empty circles indicate measured and simulated results, respectively. (d) Power density variation of the PME to incident polarization angles. (e) Calculated cooling temperature of the PME as a function of the non-radiative coefficient. (f) Calculated temperature of the PME as a function of ambient temperature.

calculation in Sec. IV). Owing to the spectral characteristics of the polarizer (i.e., low solar absorptivity and low IR emissivity), as shown in Fig. S3, the thermal radiation of the polarizer to the emitter is negligible in the simulation. The cooling temperature (T_{cool}) of the PME varies from −212 to 28 °C continuously with the variation of φ_{pol} at zero non-radiative heat exchange. The cooling temperature (T_{cool}) is the difference between the emitter temperature (T_{emit}) and the ambient temperature (T_{amb}) (i.e., $T_{amb} - T_{emit}$). This result proves the prominent heating, insulating, and cooling capabilities via a simple φ_{pol} tuning method. Moreover, the emissivity tunability of the PME shows a weak dependency on the incident angle owing to the thin thickness of the Ag layer (~100 nm) compared with the thermal wavelength (i.e., ~10 μm) (Fig. S5).

Figure 3(a) presents the cooling temperature of the PME at the co-polarized ($T_{cool,co}$) and cross-polarized ($T_{cool,cross}$) states, respectively, as a function of grid width (w_{grid}) and metal fill factor (FF = w_{grid}/P). The gray-colored region between cyan and yellow lines indicates the region in which the PME provides a superior cooling/heating performance (i.e., $T_{cool,co} > 20$ °C and $T_{cool,cross} < -20$ °C). Our optimum conditions [w_{grid} = 1 μm and fill factor (FF) = 50%] offer the widest tuning range of the temperature within that area (i.e., $T_{cool,co}$ = 23 °C and $T_{cool,cross}$ = −212 °C). The design rule for the optimized condition is shown in Fig. 3(b).

For high cooling/heating capabilities, an important aspect of the optical properties in the PME is to accomplish different absorption spectra with a high selectivity in the solar (0.28–2.5 μm) and the MIR regions (8–13 μm) under cooling and heating modes. This means that the PME should provide a higher absorptivity in the MIR ($\varepsilon_{MIR,co}$) than in the solar region ($A_{solar,co}$) at the co-polarized state (φ_{pol} = 0°) for radiative cooling. In contrast, the PME should satisfy the opposite conditions (i.e., $\varepsilon_{MIR,cross} < A_{solar,cross}$) at the cross-polarized state (φ_{pol} = 90°) for solar heating. Hence, it is essential to achieve both a large emissivity gap between two different states ($\Delta\varepsilon_{MIR} = \varepsilon_{MIR,co} - \varepsilon_{MIR,cross}$) and a small solar absorptivity gap ($\Delta A_{solar} = A_{solar,co} - A_{solar,cross}$). As the metal grid width increases with a fixed fill factor (50%), the period of the metal grid exceeds the subwavelength dimension, weakening polarization dependency (i.e., decrease in $\Delta\varepsilon_{MIR}$ and ΔA_{solar}), as shown in Fig. 3(b) (left) and Fig. S6(a). With increasing fill factor under the same metal width (1 μm), the PME provides shorter subwavelength periods, resulting in larger emissivity/absorptivity differences [Fig. 3(b) (right) and Fig. S6(b)]. Consequently, the optimized PME (i.e., w_{grid} = 1 μm and FF = 50%) presents a large emissivity gap with a small solar absorption change (i.e., $\Delta\varepsilon_{MIR}$ ~ 75% and ΔA_{solar} ~ 2%), as depicted in Fig. 3(c). The metal layer thickness of 100 nm comprises the broad temperature variation of the system (Fig. S7).

Figure 3(d) shows the cooling power of the PME (P_{cool}) as a function of φ_{pol}. The PME possesses a continuous cooling power from −17 to 51 W/m^2 by varying the polarization angle. The higher the polarization angle, the lower the P_{rad} and P_{atm} under consistent P_{Sun} owing to a relatively larger $\Delta\varepsilon_{MIR}$ than ΔA_{solar}, resulting in the multi-state cooling power. The fraction of the thermal radiation and solar absorption intensities under different polarization angles is presented in Fig. S8. Figure 3(e) shows the calculated cooling temperatures at the co-polarized and the cross-polarized states, in terms of non-radiative heat exchange coefficient, h_c. The temperature modulation ability degrades with increasing h_c. Nevertheless, the PME provides a broad temperature variation

(ΔT_{cool} > 5 °C) in practical situations (i.e., h_c > 5). Meanwhile, the average U.S. household spends $35 per month for lowering/raising the inner temperature by 5 °C,[48] indicating that the PME sufficiently can reduce the energy cost. Figure 3(f) represents the increase in the emitter temperature gap (ΔT_{emit}) between the co-polarized and the cross-polarized states as a function of ambient temperature. The temperature gap rises from 7.8 to 16.8 °C as the ambient temperature increases (from 270 to 330 K). Since cooling is mostly demanded in hot weather (T_{amb} > 300 K), this property is beneficial for energy saving in practical cases.

As a proof-of-concept demonstration, we measured the temperatures of two fabricated samples outdoors to verify the cooling performance with respect to polarization angle variation [Fig. 4(a)]. The temperature of the sample is measured during the polarizer rotation for variable emission, and the other is exposed to the sky without a polarizer for single-state emission as a control group. Figure S9 displays the photograph of the used outdoor measurement setup. The emitter and the polarizer are placed at a short distance (~5 cm) to avoid the conduction effect that weakens the cooling/heating effect of the PME. Figure 4(b) shows the cooling temperatures of the PME at three different polarization states (i.e., φ_{pol} = 0, 45, and 90°), in terms of non-radiative coefficient and ambient air temperature. This result indicates that the PME provides an extended cooling temperature range with a higher ambient temperature. In addition, the cooling temperature trends agree with the calculation trends.

Figure 4(c) presents the real-time temperature measurement for two samples. The temperatures of samples are recorded under a sunshade to observe the effect of emissivity variation. As expected, the conventional system (w/o polarizer) only lowers the temperature, yielding excess cooling below the target temperature (17–18 °C). As for the proposed system, the IR polarizer first aligns with the same axis of the PME (i.e., φ_{pol} = 0°) to cool the objects at a high ambient temperature (i.e., 18–20 °C). During ambient temperature drops, the polarizer rotates with the polarization angle of 45° at 13:40 to prevent from overcooling below 17 °C. When the ambient temperature drops again, the polarizer blocks the thermal emission from the PME to raise the temperature by cross-axis alignment at 14:46. Accordingly, the PME with the IR polarizer can maintain the temperature within the target range (17–18 °C), while the conventional setup (w/o IR polarizer) leads to overcooling below 17 °C. This result proves the outstanding thermal regulation property of the proposed system. Moreover, our system can maintain a constant temperature even in cold weather (T_{amb} ~ 4 °C), demonstrating a broad operating temperature range of the PME (Fig. S10). We targeted different temperature ranges in the measurements to maintain the emitter's temperature near the ambient temperature. This property extends to applications that require low-temperature regulation, including refrigerator trucks and food storage. Figure S11 describes the measured solar irradiance during the measurements in Fig. 4(c). The solar irradiance does not affect the emitter temperature during the measurement owing to the sunshade. Figure 4(d)

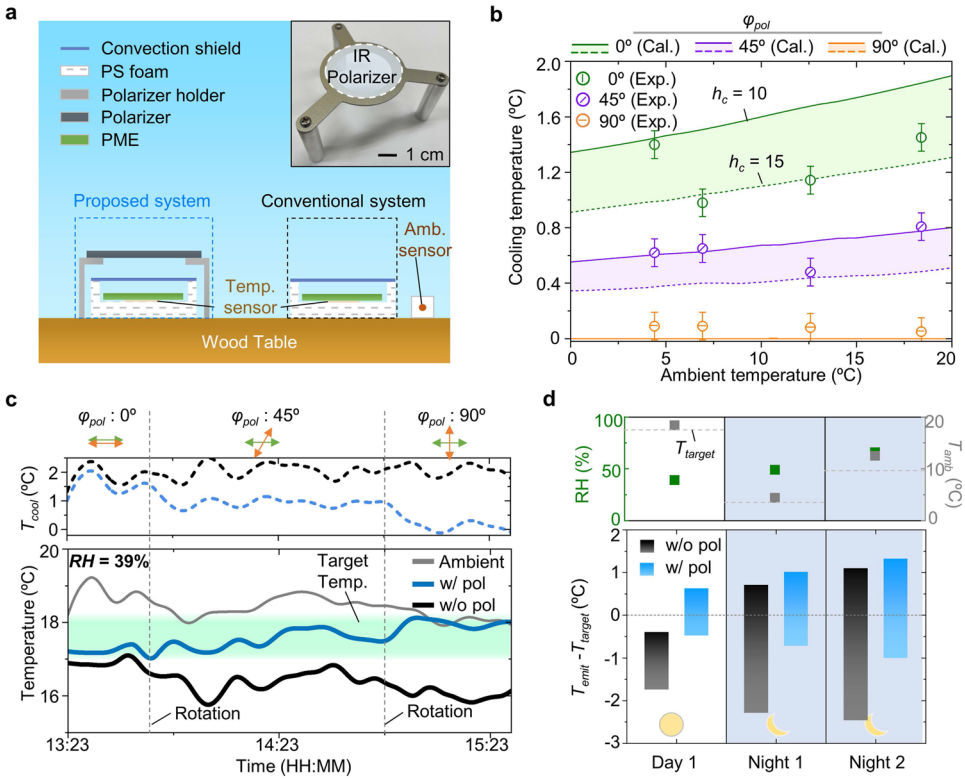

FIG. 4. (a) Schematic of the outdoor measurement setup with an IR polarizer. (b) Calculated cooling temperatures of the proposed system as a function of ambient temperature. The empty circles indicate the experimental results. (c) Real-time temperature measurement of the system under varying ambient temperatures. (d) Temperature variations for three days with different values of ambient temperature and humidity.

presents the repeated measurement results under different values of relative humidity and ambient temperature. Our proposed system provides a notable thermoregulation performance in all days compared with the conventional system (i.e., no polarizer). These results prove that introducing a polarizer enables maintaining the temperature near the targeted region effectively in all weather conditions. The substrate used in the thermal emitter can replace other polymers (i.e., PDMS and PET) with various benefits, such as cost and emissivity. Moreover, the IR polarizer can be fabricated by using BaF_2 and polyethylene as substrates (Fig. S12). Owing to the benefits of low material cost and easy fabrication process, using a polymer substrate significantly decreases the overall cost, allowing practical applications, including on roofs and trucks.

III. CONCLUSION

This study proposed an innovative strategy to construct a radiation-based simple temperature regulator utilizing a linearly polarized thermal emitter and an IR polarizer. The PME facilitates the continuous modulation of the emissivity from 2% to 80% by the in-plane rotation of IR polarizer. Theoretical simulations spectrally design the optimum PME and thermally reveal the continuous heating/cooling performance (−17 to 51 W/m^2). In addition, the PME provides a broad range of temperature modulation capability ($\Delta T_{emit} \sim 5\,^{\circ}C$) at $h_c = 10$ $W/m^2/K$, indicating a practical situation. This advantage can save the energy consumed for thermoregulation by over 20 GJ compared to single- and dual-state emitters across all different climate zones. The outdoor measurements proved the notable temperature adjustment capability of the proposed system in various weather conditions. The immediate rotation against the ambient temperature of the polarizer enables maintaining the temperature within 0.5 °C from the target temperature, whereas the conventional emitter (single-state emission) exceeds ~2 °C from the desired temperature. These successful demonstrations indicate that the fine tunability of emissivity and broad operating temperature enables a wide application range from million cubic meters of massive structures (e.g., buildings and vehicles) to centimeter-scale small electronic devices in all weather conditions. In future work, we expect that developing polarization dependency of solar absorption would improve the heating/cooling performance of the PME.

IV. METHODS

Optical simulation for spectral results: To simulate the emissivity spectra of the PME, rigorous coupled wave analysis-based commercial software (DiffractMOD, RSoft Design Group, Synopsys, USA) was employed. In addition, absorption profiles were simulated using the same software. In all the simulations, a 1 nm-square grid size was exploited to obtain a stable emissivity. The complex refractive index dispersions for materials (i.e., SiO_2 and BaF_2) were considered to obtain accurate spectral results. The refractive indices were obtained from previously published results.[49,50] The Drude model was used for the optical constants of Ag.

Building energy saving performance simulation: The heating and cooling energies are modeled from whole building energy simulation using a commercial software (EnergyPlus). Three different emitters (i.e., single-, dual-, and multi-state), applied on the exterior surface of the building roof, were utilized for the energy saving simulation of the heating, ventilation, and air-conditioning (HVAC) systems. In the simulation, a one-story medium-sized office building model is exploited (Fig. S1), which is a Department of Energy (DOE) commercial reference building satisfying the insulation model of American Society of Heating, Refrigerating and Air Conditioning Engineers (ASHRAE) standard 90.1-2016.[51] Several climate data were used for simulation from the typical meteorological year (TMY3) weather data.[46] The detailed parameters for the simulation (i.e., absorptivity of roof, building area, and temperature setpoint) are summarized in Table S2.

Fabrication of the PME: A clean quartz substrate was prepared, and a positive photoresist (PR; AZ5214E, MicroChemicals, Germany) was spin-coated at 4000 rpm for 30 s. The sample was then baked at 90 °C for 60 s as a soft bake step. To achieve a high resolution, a stepper (i-line stepper, NSR-2205i11D, Nikon Inc., Japan) was used with a 1D micro-grating mask under an exposure intensity of 11 mW/cm^2 for 5 s. After the exposure, the sample was then developed by immersing a developer (AZ-MIF-300, MicroChemicals, Germany) for 60 s. Hard-baking was also performed at 110 °C for 120 s. Then, a 100 nm-thick Ag layer was deposited using a magnetron radio-frequency sputtering system (DDHT-LSH2, Daedong High Tech., Ltd., Korea) under a high vacuum (≈10^{-6} Torr). After the metal deposition, lift-off was performed to reveal each patterned area.

Structural and spectral analyses of the fabricated samples: The absorptivity spectra were characterized with an integrating sphere over the wavelength range of 280–2500 nm using an ultraviolet–visible–near-infrared (UV–vis–NIR) spectrometer (Lambda 950, Perkin Elmer, Inc., USA). Additionally, the emissivity spectra for mid-infrared (MIR) regions were analyzed using a Fourier transform infrared spectrometer (VERTEX 70v, Bruker, USA) with an Au-coated integrating sphere. The emissivity spectra were evaluated from the measured reflectance and transmittance spectra (i.e., E = 100 − R − T). A SEM (S-4700, Hitachi Hi-Technologies, Japan) was utilized to observe the top and cross section of the fabricated sample. To measure the emissivity with the variation of the polarization angle, a commercial IR polarizer (WP50H-K, Thorlabs, USA) was utilized for calibration.

Thermal equilibrium equation: The thermal equilibrium equation, $P_{rad}(T_{emit}) - P_{Sun} - P_{atm}(T_{ambient}) + P_{non-rad} = 0$, is composed of the following four terms:

$$P_{rad}(T_{emit}) = \int_0^{2\pi}\int_0^{\frac{\pi}{2}}\int_0^{\infty} I_{BB}(T_{emit},\lambda)\varepsilon(\lambda,\theta) \times \cos(\theta)\sin(\theta)d\lambda d\theta d\phi, \quad (1)$$

$$P_{atm}(T_{ambient}) = \int_0^{2\pi}\int_0^{\pi/2}\int_0^{\infty} I_{BB}(T_{ambient},\lambda)\varepsilon(\lambda,\theta)\varepsilon_{amb}(\lambda,\theta) \times \cos(\theta)\sin(\theta)d\lambda d\theta d\phi, \quad (2)$$

$$P_{sun} = \int_0^{\infty} I_{AM1.5G}(\lambda)\varepsilon(\lambda,\theta)d\lambda, \quad (3)$$

$$P_{non-rad} = h_c(T_{emit} - T_{ambient}). \quad (4)$$

where $\varepsilon(\lambda,\theta)$ is the angular emissivity of emitter; $I_{BB} = (2h_c c^2/\lambda^5)/[e^{\frac{h_c}{\lambda k_B T}} - 1]$ is the spectral radiance of a blackbody at temperature T; and h, c, k_B, λ, and h_c are Planck's constant,

the velocity of light, the Boltzmann constant, wavelength, and the non-radiative heat exchange coefficient, respectively. The atmospheric emissivity is given by $\varepsilon_{amb}(\lambda,\theta) = 1 - t(\lambda)^{1/\cos(\theta)}$, where t is the sky transmission of Mauna Kea atmospheric transmission.[52] In this study, we calculated the cooling performance of an integrated system with a polarizer and PME. The emissivities of the system at p-polarization and s-polarization states ($\varepsilon_{p-pol.}$ and $\varepsilon_{s-pol.}$) can be obtained by the generalized Malus law as follows:[53]

$$\varepsilon_{p-pol.} = \varepsilon_{emit,p-pol.} \times T_{pol,p-pol.}\cos^2(\varphi_{pol}), \tag{5}$$

$$\varepsilon_{s-pol.} = \varepsilon_{emit,s-pol.} \times T_{pol,s-pol.}\sin^2(\varphi_{pol}), \tag{6}$$

where $\varepsilon_{emit,\,p\text{-}pol.}$ is the emitter emissivity at the p-polarization state and $\varepsilon_{emit,\,s\text{-}pol.}$ is the emitter emissivity at the s-polarization state and $T_{pol,\,p\text{-}pol}$ and $T_{pol,\,s\text{-}pol}$ are the transmittance of the IR polarizer at p-polarization and s-polarization states, respectively. From the definition of electromagnetic wave, the polarization-averaged emissivity ($\varepsilon_{avg.}$) can be written as

$$\varepsilon_{avg.}(\lambda,\theta,\varphi_{pol}) = \frac{1}{2}\left(T_{pol,p-pol.}\varepsilon_{emit,p-pol.}\cos^2(\varphi_{pol}) + T_{pol,s-pol.}\varepsilon_{emit,s-pol.}\sin^2(\varphi_{pol})\right). \tag{7}$$

The term $\varepsilon_{avg.}(\lambda,\theta,\varphi_{pol})$ replaces $\varepsilon(\lambda,\theta)$ in Eqs. (1)–(3) to confirm the dependence on the polarization angle (φ_{pol}).

Measurements of thermal imaging and cooling performance: For thermal imaging, the PME was placed on a hot plate at a temperature of 50 °C. The IR polarizer with a holder was placed above the sample with a distance of 1 cm. A thermal camera (E6, FLIR Systems, Inc., USA) captured the sample surface with rotating the IR polarizer. For the real-time temperature measurement, temperature sensors (ST-50, RKC Instrument Inc., Japan) were inserted between the samples and styrofoam. The inserted sensors were connected to a data logger (RDXL6SD, Omega Engineering, USA). The ambient air temperature sensor was exploited to measure the temperature of the naturally convective air.

SUPPLEMENTARY MATERIAL

See supplementary material for additional details about the simulations and experimental results on characterization and cooling performance of the PME.

ACKNOWLEDGMENTS

This work was supported by the GIST Research Institute (GRI) RISE, GIST-MIT Research Collaboration, Startup Acceleration Center, and AI-based GIST Research Scientist Project through a grant funded by the GIST and National Research Foundation of Korea (NRF) funded by the Ministry of Science and ICT (Grant Nos. NRF-2021M3H4A1A04086552, NRF2018M3D1A1058997, NRF-2022M3H4A1A02046445, 2022M3C1A3081312, and NRF-2021R1C1C2013605). This research was also supported by 2022 BK21 FOUR Program of Pusan National University. This research was supported by Nano·Material Technology Development Program through the National Research Foundation of Korea (NRF) funded by the Ministry of Science, ICT and Future Planning (2009-0082580).

AUTHOR DECLARATIONS

Conflict of Interest

The authors have no conflicts to disclose.

Author Contributions

Do Hyeon Kim: Conceptualization (equal); Data curation (lead); Formal analysis (lead); Investigation (equal); Methodology (equal); Resources (equal); Validation (equal); Visualization (lead); Writing – original draft (equal); Writing – review & editing (equal). **Se-Yeon Heo**: Data curation (supporting); Validation (supporting); Visualization (supporting); Writing – review & editing (supporting). **Yeon-Wha Oh**: Methodology (supporting); Resources (equal). **Sanghee Jung**: Methodology (supporting); Resources (equal). **Min Hyung Kang**: Conceptualization (equal); Data curation (supporting); Investigation (supporting); Resources (supporting). **Il-Suk Kang**: Methodology (equal); Resources (equal); Writing – review & editing (supporting). **Gil Ju Lee**: Conceptualization (equal); Data curation (equal); Formal analysis (supporting); Investigation (supporting); Methodology (supporting); Project administration (supporting); Supervision (equal); Visualization (supporting); Writing – review & editing (equal). **Young Min Song**: Conceptualization (equal); Funding acquisition (equal); Methodology (equal); Project administration (equal); Resources (equal); Software (equal); Supervision (equal); Validation (equal); Visualization (equal); Writing – review & editing (equal).

DATA AVAILABILITY

The data that support the findings of this study are available from the corresponding authors upon reasonable request.

REFERENCES

[1] L. T. Biardeau, L. W. Davis, P. Gertler, and C. Wolfram, "Heat exposure and global air conditioning," Nat. Sustainability **3**(1), 25 (2020).
[2] R. Alcalá, J. Alcalá-Fdez, M. J. Gacto, and F. Herrera, "Improving fuzzy logic controllers obtained by experts: A case study in HVAC systems," Appl. Intell. **31**(1), 15 (2009).
[3] S. Sotoma, C. Zhong, J. C. Y. Kah, H. Yamashita, T. Plakhotnik, Y. Harada, and M. Suzuki, "In situ measurements of intracellular thermal conductivity using heater-thermometer hybrid diamond nanosensors," Sci. Adv. **7**(3), eabd7888 (2021).
[4] S. Hong, Y. Gu, J. K. Seo, J. Wang, P. Liu, Y. S. Meng, S. Xu, and R. Chen, "Wearable thermoelectrics for personalized thermoregulation," Sci. Adv. **5**(5), eaaw0536 (2019).
[5] R. A. Kishore, A. Nozariasbmarz, B. Poudel, M. Sanghadasa, and S. Priya, "Ultra-high performance wearable thermoelectric coolers with less materials," Nat. Commun. **10**(1), 1765 (2019).
[6] B. Russ, A. Glaudell, J. J. Urban, M. L. Chabinyc, and R. A. Segalman, "Organic thermoelectric materials for energy harvesting and temperature control," Nat. Rev. Mater. **1**(10), 16050 (2016).

[7]Y. Fang, G. Chen, M. Bick, and J. Chen, "Smart textiles for personalized thermoregulation," Chem. Soc. Rev. **50**, 9357 (2021).
[8]J. Palmer, N. Terry, and P. Pope, "How much energy could be saved by making small changes to everyday household behaviours," A report for department of energy and climate change, 2012.
[9]A. P. Raman, M. A. Anoma, L. Zhu, E. Rephaeli, and S. Fan, "Passive radiative cooling below ambient air temperature under direct sunlight," Nature **515**(7528), 540 (2014).
[10]J. Mandal, Y. Fu, A. C. Overvig, M. Jia, K. Sun, N. N. Shi, H. Zhou, X. Xiao, N. Yu, and Y. Yang, "Hierarchically porous polymer coatings for highly efficient passive daytime radiative cooling," Science **362**(6412), 315 (2018).
[11]X. Li, B. Sun, C. Sui, A. Nandi, H. Fang, Y. Peng, G. Tan, and P.-C. Hsu, "Integration of daytime radiative cooling and solar heating for year-round energy saving in buildings," Nat. Commun. **11**(1), 6101 (2020).
[12]Y. Zhai, Y. Ma, S. N. David, D. Zhao, R. Lou, G. Tan, R. Yang, and X. Yin, "Scalable-manufactured randomized glass-polymer hybrid metamaterial for daytime radiative cooling," Science **355**(6329), 1062 (2017).
[13]D. H. Kim, G. J. Lee, S.-Y. Heo, S. Son, K. M. Kang, H. Lee, and Y. M. Song, "Ultra-thin and near-unity selective emitter for efficient cooling," Opt. Express **29**(20), 31364 (2021).
[14]E. A. Goldstein, A. P. Raman, and S. Fan, "Sub-ambient non-evaporative fluid cooling with the sky," Nat. Energy **2**(9), 17143 (2017).
[15]D. Zhao, A. Aili, Y. Zhai, J. Lu, D. Kidd, G. Tan, X. Yin, and R. Yang, "Subambient cooling of water: Toward real-world applications of daytime radiative cooling," Joule **3**(1), 111 (2019).
[16]S. Son, T. Y. Lee, D. Chae, H. Lim, J. Ha, Y. K. Kim, and H. Lee, "Efficient daytime radiative cooling cover sheet with dual-modal optical properties," Adv. Opt. Mater. **10**, 2201771 (2022).
[17]D. Li, X. Liu, W. Li, Z. Lin, B. Zhu, Z. Li, J. Li, B. Li, S. Fan, and J. Xie, "Scalable and hierarchically designed polymer film as a selective thermal emitter for high-performance all-day radiative cooling," Nat. Nanotechnol. **16**(2), 153 (2021).
[18]L.-C. Hu, C.-H. Xue, B.-Y. Liu, X.-J. Guo, J.-H. Wang, and F.-Q. Deng, "Scalable superhydrophobic flexible nanofiber film for passive daytime radiative cooling," ACS Appl. Polym. Mater. **4**, 3343 (2022).
[19]R. Xiao, C. Hou, W. Yang, Y. Su, Y. Li, Q. Zhang, P. Gao, and H. Wang, "Infrared-radiation-enhanced nanofiber membrane for sky radiative cooling of the human body," ACS Appl. Mater. Interfaces **11**(47), 44673 (2019).
[20]X. Zhang, L. Yang, F. Wang, Z. Cheng, and H. Liang, "Wrinkled surface microstructure for enhancing the infrared spectral performance of radiative cooling," Opt. Express **29**(8), 11416 (2021).
[21]Z. Cheng, F. Wang, H. Wang, H. Liang, and L. Ma, "Effect of embedded polydisperse glass microspheres on radiative cooling of a coating," Int. J. Therm. Sci. **140**, 358 (2019).
[22]Y. Shi, W. Li, A. Raman, and S. Fan, "Optimization of multilayer optical films with a memetic algorithm and mixed integer programming," ACS Photonics **5**(3), 684 (2017).
[23]D. Chae, S. Son, Y. Liu, H. Lim, and H. Lee, "High-performance daytime radiative cooler and near-ideal selective emitter enabled by transparent sapphire substrate," Adv. Sci. **7**(19), 2001577 (2020).
[24]B. Zhu, W. Li, Q. Zhang, D. Li, X. Liu, Y. Wang, N. Xu, Z. Wu, J. Li, and X. Li, "Subambient daytime radiative cooling textile based on nanoprocessed silk," Nat. Nanotechnol. **16**(12), 1342 (2021).
[25]P.-C. Hsu, C. Liu, A. Y. Song, Z. Zhang, Y. Peng, J. Xie, K. Liu, C.-L. Wu, P. B. Catrysse, and L. Cai, "A dual-mode textile for human body radiative heating and cooling," Sci. Adv. **3**(11), e1700895 (2017).
[26]S. Y. Heo, D. H. Kim, Y. M. Song, and G. J. Lee, "Determining the effectiveness of radiative cooler-integrated solar cells," Adv. Energy Mater. **12**(10), 2103258 (2022).
[27]L. Zhu, A. Raman, K. X. Wang, M. A. Anoma, and S. Fan, "Radiative cooling of solar cells," Optica **1**(1), 32 (2014).
[28]M. H. Kang, G. J. Lee, J. H. Lee, M. S. Kim, Z. Yan, J. W. Jeong, K. I. Jang, and Y. M. Song, "Outdoor-useable, wireless/battery-free patch-type tissue oximeter with radiative cooling," Adv. Sci. **8**(10), 2004885 (2021).
[29]H. Zhang and D. Fan, "Improving heat dissipation and temperature uniformity in radiative cooling coating," Energy Technol. **8**(5), 1901362 (2020).
[30]T. Li, Y. Zhai, S. He, W. Gan, Z. Wei, M. Heidarinejad, D. Dalgo, R. Mi, X. Zhao, and J. Song, "A radiative cooling structural material," Science **364**(6442), 760 (2019).
[31]K. Zhang, D. Zhao, X. Yin, R. Yang, and G. Tan, "Energy saving and economic analysis of a new hybrid radiative cooling system for single-family houses in the USA," Appl. Energy **224**, 371 (2018).
[32]P.-C. Hsu and X. Li, "Photon-engineered radiative cooling textiles," Science **370**(6518), 784 (2020).
[33]S.-Y. Heo, G. J. Lee, D. H. Kim, Y. J. Kim, S. Ishii, M. S. Kim, T. J. Seok, B. J. Lee, H. Lee, and Y. M. Song, "A janus emitter for passive heat release from enclosures," Sci. Adv. **6**(36), eabb1906 (2020).
[34]D. H. Kim, G. J. Lee, S.-Y. Heo, I.-S. Kang, and Y. M. Song, "Thermostat property of janus emitter in enclosures," Sol. Energy Mater. Sol. Cells **230**, 111173 (2021).
[35]H. Zhai, D. Fan, and Q. Li, "Dynamic radiation regulations for thermal comfort," Nano Energy **100**, 107435 (2022).
[36]J. Mandal, M. Jia, A. Overvig, Y. Fu, E. Che, N. Yu, and Y. Yang, "Porous polymers with switchable optical transmittance for optical and thermal regulation," Joule **3**(12), 3088 (2019).
[37]X. A. Zhang, S. Yu, B. Xu, M. Li, Z. Peng, Y. Wang, S. Deng, X. Wu, Z. Wu, and M. Ouyang, "Dynamic gating of infrared radiation in a textile," Science **363**(6427), 619 (2019).
[38]H. Zhao, Q. Sun, J. Zhou, X. Deng, and J. Cui, "Switchable cavitation in silicone coatings for energy-saving cooling and heating," Adv. Mater. **32**(29), 2000870 (2020).
[39]Q. Zhang, Y. Lv, Y. Wang, S. Yu, C. Li, R. Ma, and Y. Chen, "Temperature-dependent dual-mode thermal management device with net zero energy for year-round energy saving," Nat. Commun. **13**(1), 4874 (2022).
[40]W. Wang, Q. Zou, N. Wang, B. Hong, W. Zhang, and G. P. Wang, "Janus multilayer for radiative cooling and heating in double-side photonic thermal system," ACS Appl. Mater. Interfaces **13**(36), 42813 (2021).
[41]X. Liu, Y. Tian, F. Chen, A. Ghanekar, M. Antezza, and Y. Zheng, "Continuously variable emission for mechanical deformation induced radiative cooling," Commun. Mater. **1**(1), 95 (2020).
[42]S. Wang, T. Jiang, Y. Meng, R. Yang, G. Tan, and Y. Long, "Scalable thermochromic smart windows with passive radiative cooling regulation," Science **374**(6574), 1501 (2021).
[43]K. Tang, K. Dong, J. Li, M. P. Gordon, F. G. Reichertz, H. Kim, Y. Rho, Q. Wang, C.-Y. Lin, and C. P. Grigoropoulos, "Temperature-adaptive radiative coating for all-season household thermal regulation," Science **374**(6574), 1504 (2021).
[44]M. Kim, D. Lee, Y. Yang, and J. Rho, "Switchable diurnal radiative cooling by doped VO_2," Opto-Electron. Adv. **4**(5), 05200006 (2021).
[45]M. Ono, K. Chen, W. Li, and S. Fan, "Self-adaptive radiative cooling based on phase change materials," Opt. Express **26**(18), A777 (2018).
[46]Typical Meteorological Year 3 (National Solar Radiation Data Base, 1991-2005 2020), Vol. 2020, https://nsrdb.nrel.gov/.
[47]K. H. Khan, C. Ryan, and E. Abebe, "Optimizing HVAC energy usage in industrial processes by scheduling based on weather data," IEEE Access **5**, 11228 (2017).
[48]Office of Energy Saver, Heating and Cooling US Department of Energy https://www.energy.gov/energysaver/heating-and-cooling.
[49]S. Popova, T. Tolstykh, and V. Vorobev, "Optical characteristics of amorphous quartz in the 1400−200 cm^{-1} region," Opt. Spectrosc. **33**, 444 (1972).
[50]H. H. Li, "Refractive index of alkaline earth halides and its wavelength and temperature derivatives," J. Phys. Chem. Ref. Data **9**(1), 161 (1980).
[51]Energy standard for building except low-rise residential buildings, https://www.ashrae.org/file%20library/technical%20resources/standards%20and%20guidelines/ standards%20addenda /90.1-2016/90_1_2016_m_ai_aj_au_az_bg_dn_20210324.pdf.
[52]M. G. Burton, J. S. Lawrence, M. C. B. Ashley, J. A. Bailey, C. Blake, T. R. Bedding, J. Bland-Hawthorn, I. A. Bond, K. Glazebrook, and M. G. Hidas, "Science programs for a 2-m class telescope at dome C, Antarctica: PILOT, the pathfinder for an international large optical telescope," Publ. Astron. Soc. Aust. **22**(3), 199 (2005).
[53]I. Damian, "Malus' law for a real polarizer," arXiv:physics/0604073 (2006).